Circuit Model in Design of THz Transparent Electrodes Based on Two-Dimensional Arrays of Metallic Square Holes

Ghazaleh Kafaie Shirmanesh, Elahe Yarmoghaddam, Amin Khavasi, and Khashayar Mehrany

***Abstract*—In this paper, we propose a circuit model for two-dimensional arrays of metallic square holes located on a homogeneous substrate, in order to propose a new scheme containing this type of metamaterials to obtain transparent electrodes with simultaneous terahertz transparency and low electrical resistance. The results of the introduced circuit model, which is a fully analytical model with explicit expressions, are in almost complete agreement with the full-wave simulations. Thanks to this analytical model, we can employ standard binomial matching transformer in order to minimize the reflected power from the structure at a desired frequency. Furthermore, taking advantage of this model, we design an optimized tri-layer structure by seeking for a high optical transmittance at the desired frequency and over a wide bandwidth. The obtained transparent electrode has a high power transmission (more than 85%) within a wide frequency range (48% of the central frequency) which is desirable in commonly used transparent electrodes. The square holes are perforated in thick metallic slabs which drastically reduce the electrical resistance of the structure.**

***Index Terms*—Circuit model, metamaterial, transparent conductive electrodes (TCEs).**

I. Introduction

TRANSPARENT conducting electrodes (TCEs) with simultaneous high optical transmission and low electrical resistivity are required in many optoelectronic and electrooptic applications such as touch panels, photovoltaic cells, smart windows, LEDs, and LCDs [1]. Nowadays, the most commonly used material for TCEs is indium–tin–oxide (ITO) [2]. Although it shows satisfying electrical and optical properties, ITO comes with some inherent limitations. The brittle nature of ITO leads to failure of this class of electrodes to be used in flexible applications such as electronic papers or flexible screens [3]. In addition, the scarcity and continuous increase in the price of indium, which is the main component of ITO, its susceptibility to ion diffusion into organic layers, and its relatively low transmittance in the blue region is of great concern for an eventual implementation in the everyday devices [4], [5], and [6]. The most important limitation of ITO is an inherent tradeoff between the optical properties and the electrical ones [7]. Thick ITO films offer lower sheet resistance, but this comes at the expense of lower optical transmittance and vice versa [8], [9]. In recent research efforts, carbon nanotube networks [10] and unpatterned thin metal films [11] have been evaluated as potential replacements for the conventional ITO electrodes. However, these TCEs still suffer from the classic tradeoff between the optical transmittance and electrical conductivity [12]. An increase in the thickness of the film results in a lower electrical sheet resistance due to the increase in the number of charge carriers, which improves the electrical performance. On the other hand, it increases the amount of light absorbed inside the film and lowers the optical transmittance, which degrades the optical performance. Recently, graphene, the one-atom-thick two-dimensional (2-D) allotrope of carbon [13], is attracting scientific attentions to be used as transparent electrode [14]. Nevertheless, there is also a tradeoff between the optical transmission of graphene and its achievable electrical conductivity [15]. In the THz regime, the transmittance of the conventional transparent electrodes drops even further and the aforementioned tradeoff between the transmittance and the electrical resistance of the electrodes becomes severe [16].

Recently, the need for simultaneous high transparency and good electrical conductivity is addressed by using micro-structured metallic meshes, i.e., by a geometrical transformation of the metal film [17]. In this manner, acceptable level of transparency can be reached even at THz frequencies. In the mentioned scheme, a composite layer consisting of two differently shaped metallic meshes filled with silica, and a silica layer as a spacer between them is placed on top of a semi-infinite Si substrate. The obtained structure makes a continuous plasmonic metal film, on top of a semi-infinite substrate, transparent at certain frequency windows over narrow bandwidths (7.5% of central frequency for power transmission of more than 85%). The in-plane conductivity of this scheme, however, is limited because the thickness of the holes is very small ($\sim$ 200 nm).

Here, we propose a new metamaterial-based TCE with significantly improved bandwidth (48% of the central frequency). Moreover, the proposed metallic structure used for our TCE is very thick (10 μm) leading to excellent in-plane conductivity.

We can achieve the desired electrode with high optical transparency by employing a micro-structured 2-D arrays of square holes, while guaranteeing the electrode's high electrical conductivity by perforating the mentioned holes in thick metal

Manuscript received October 15, 2013; revised February 14, 2014; accepted March 07, 2014. Date of publication April 14, 2014; date of current version April 29, 2014.

The authors are with the Electrical Engineering Department, Sharif University of Technology, Tehran 11155-4363, Iran (e-mail: kafaie@ee.sharif.edu; e_yarmoghaddam@ee.sharif.edu; khavasi@sharif.edu; mehrany@sharif.edu).

Color versions of one or more of the figures in this paper are available online at http://ieeexplore.ieee.org.

Digital Object Identifier 10.1109/TTHZ.2014.2313956

slabs. In order to efficiently design the structure, we propose a fully analytical circuit model in the subwavelength regime characterized by explicit expressions for the mentioned array of square holes placed on a homogeneous substrate. In the proposed circuit model, the bulk of the hole array is replaced by a transmission line, and a surface admittance is used to model the interface between the 2-D metallic array and an arbitrary homogeneous medium. The admittance and the propagation constant of the bulk are obtained by considering the fundamental eigenmode of the electromagnetic wave inside the metallic holes, and the surface admittances are obtained by applying the mode matching technique, in which the fundamental mode inside the holes is only considered, at the boundaries.

Taking advantage of the analytical nature of the proposed circuit model, we design an optimized structure with almost complete power transmission at a desired frequency and high level of transmittance over a wide frequency range. The performance of the structure can be further enhanced by inserting additional layers. Such an optimized design is almost impossible by employing time-consuming conventional full-wave simulation techniques.

The remainder of this paper is organized as follows. Section II introduces the proposed circuit model whose limitations are expounded in the next section. The designed structures and the corresponding simulation results are presented in Section IV, and Section V concludes the paper.

II. Circuit Model

Here, an analytical circuit model for 2-D arrays of square holes with nonzero thickness is proposed. Previously, equivalent circuit models have been presented for zero thickness screens of ideally conducting square meshes located in a homogeneous host medium [18]. However, to the best of our knowledge, no fully analytical circuit model is presented for nonzero thickness hole arrays.

Consider a 2-D periodic array of metallic square holes filled with a homogeneous medium with permittivity and permeability represented by ε_2 and μ_2, respectively. The semi-infinite metallic structure is covered from top by a medium with the permittivity, permeability and, refractive index of ε_1, μ_0, and n_1. The hole array periodicity in both $\hat{x}$ and $\hat{y}$ directions and metal line width are denoted by d and W, respectively. The structure is depicted in Fig. 1(a), and Fig. 1(b) shows the top-view of the metallic array.

In the proposed circuit model, diagrammed in Fig. 2, the cover medium is modeled by a transmission line with the characteristic admittance and propagation constant denoted by Y_1 and k_z, respectively. The bulk of the periodic metallic structure is as well replaced by a transmission line with characteristic admittance and propagation constant of Y_2 and β_2. Moreover, the interface between the metallic grating and the cover is modeled by a surface admittance donated by Y_s. This admittance represents the energy stored in the evanescent higher order diffracted waves excited due to the periodicity of the structure. In order to find the surface admittance, we employ a mode-matching technique at the discontinuity plane to obtain zeroth-order reflection coefficient from the hole array. Afterwards, by comparing the

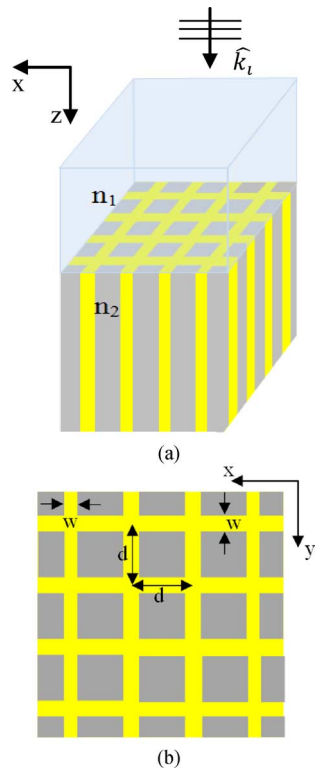

Fig. 1. (a) A 2-D array of square holes covered by a homogeneous medium. (b) Top view of the hole array.

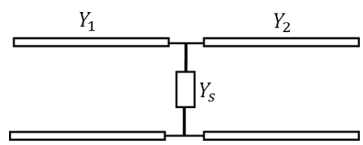

Fig. 2. Proposed circuit model for the hole array shown in Fig. 1(a).

obtained reflection coefficient with the reflection corresponding to the proposed circuit model, we can extract Y_s.

Assume that the structure is illuminated by a TM polarized wave whose wave-vector is in x-z plane. The magnetic and tangential electric fields of the incident wave are given by (the time dependence of $e^{j\omega t}$ is assumed here)

$$H_y^{\text{inc}} = H_1 e^{-jk_x x} e^{-jk_z z} \tag{1a}$$

$$E_x^{\text{inc}} = H_1 \frac{k_z}{\omega\varepsilon_1} e^{-jk_x x} e^{-jk_z z} \tag{1b}$$

where H_1 is a constant, $\omega = 2\pi f$ is the angular frequency with f being the frequency, and k_x and k_z are the wave-vector components in $\hat{x}$ and $\hat{z}$ directions and can be written as

$$k_x = k_0 n_1 \sin(\theta_i) \tag{2}$$

$$k_z = \sqrt{k_0^2 n_1^2 - k_x^2} \tag{3}$$

where k_0 is the free-space wavenumber, and θ_i denotes the incident angle.

Accordingly, the equivalent admittance of the cover region, Y_1, is as follows [19]:

$$Y_1 = \frac{\omega\varepsilon_1}{k_z}. \tag{4}$$

The reflected electromagnetic wave in the first region can be written as the superposition of the propagating and evanescent diffracted orders as

$$H_y^{ref} = \sum_{m=0,\pm1,\pm2,\ldots} \rho_m H_1 e^{-jk_{x,m}x} e^{jk_{z,m}z} \tag{5a}$$

$$E_x^{ref} = -\sum_{m=0,\pm1,\pm2,\ldots} \rho_m H_1 \frac{k_{z,m}}{\omega\varepsilon_1} e^{-jk_{x,m}x} e^{jk_{z,m}z} \tag{5b}$$

where the subscript m corresponds to the order of the diffracted wave, ρ_m is the reflection coefficient of the mth diffracted order, and $k_{x,m}$ and $k_{z,m}$ are the wave-vector components of the mentioned diffracted order in $\hat{x}$ and $\hat{z}$ directions, respectively, and are calculated by the following relations:

$$k_{x,m} = k_x + \frac{2m\pi}{d}; m = 0, \pm1, \pm2, \ldots \tag{6}$$

$$k_{z,m} = -jk_0 n_1 \sqrt{\left(\sin(\theta_i) + m\frac{\lambda_0}{n_1 d}\right)^2 - 1}; m = \pm1, \pm2, \ldots \tag{7}$$

and, for $m = 0$, we use (3) instead of (7). It should be emphasized that the model is for the subwavelength regime ($\lambda_0 > n_1 d$), and thus the zeroth diffracted order is propagating. As a result, the discriminant of (7) is positive for all incident angles and nonzero values of m.

Inasmuch as metals can be deemed as almost perfect electric conductors (PECs) in the THz regime, the transverse electric and magnetic fields inside the square holes, when considering the fundamental mode to dominate, read as

$$E_x^{inside} = E_2 \sin\left(\frac{\pi y}{a}\right) e^{-j\beta_2 z} \tag{8a}$$

$$H_y^{inside} = E_2 \frac{\beta_2}{\omega\mu_2} \sin\left(\frac{\pi y}{a}\right) e^{-j\beta_2 z} \tag{8b}$$

where E_2 is an unknown coefficient and can be obtained by applying boundary conditions, and β_2 is the propagation constant of the mode inside the hole and is obtained by

$$\beta_2 = \sqrt{k_0^2 \varepsilon_2 \mu_2 - \left(\frac{\pi}{a}\right)^2} \tag{9}$$

where $a = d - W$.

The characteristic admittance corresponding to the bulk of the square holes is

$$Y_2 = \frac{\beta_2}{\omega\mu_{\text{eff}}} \tag{10}$$

where $\mu_{\text{eff}} = \text{sinc}^2(k_x(a/2\pi))(8a^2/\pi^2 d^2)\mu_2$ is the effective permeability of the array [20], and for $k_x(a/2\pi) \ll 1$, $\mu_{\text{eff}} = (8a^2/\pi^2 d^2)\mu_2$.

Now, by applying the appropriate boundary conditions at the interface of metallic hole array and the cover, i.e., continuity of the tangential electric and magnetic fields as illustrated in the appendix, one can find the reflection coefficient of the zeroth diffracted order, given by (11), shown at the bottom of the page, where

$$\text{sinc}(x) = \frac{\sin(\pi x)}{\pi x} \tag{12}$$

is the Sinc function. On the other hand, the reflection coefficient from the equivalent circuit model, depicted in Fig. 2, is given by

$$R = -\rho_0 = \frac{Y_1 - (Y_2 + Y_s)}{Y_1 + (Y_2 + Y_s)} = \frac{1 - \frac{1}{Y_1}(Y_2 + Y_s)}{1 + \frac{1}{Y_1}(Y_2 + Y_s)}. \tag{13}$$

We can find the surface admittance between the metallic hole array and the cover, namely Y_s, by comparing (11) with (13) to yield

$$Y_s = j\frac{\omega\varepsilon_1}{k_0 n_1} \frac{1}{\text{sinc}^2\left(k_x \frac{a}{2\pi}\right)} \sum_{m\neq0} \frac{\text{sinc}^2\left(k_x \frac{a}{2\pi} + m\frac{a}{d}\right)}{\sqrt{\left(\sin(\theta_i) + m\frac{\lambda_0}{dn_1}\right)^2 - 1}}. \tag{14}$$

We verify the accuracy of the proposed circuit model through a numerical example, in which the results of the proposed analytical circuit model (implemented using MATLAB) are compared against the full-wave simulations carried out by CST Microwave Studio. The structure under study is illustrated in Fig. 3(a): an array of square holes filled with silica. The metals are assumed to be PEC, and the hole array is located on a semi-infinite silicon substrate and is covered by air.

The parameters of the structure, when illuminated by normal incidence, in accordance with Figs. 1(b) and 3(a) are as follows: $d = 50\ \mu$m, $W = 4\ \mu$m, $h_2 = 0.1\ \mu$m, $n_1 = 1$, $n_2 = 1.9621$ [21], and $n_3 = 3.4205$ [17]. The proposed circuit model corresponding to this structure is shown in Fig. 3(b) in which, Y_1 and Y_3 are the admittances of the first and the third regions, respectively, and can be obtained using (1) by substituting the parameters of the corresponding region. β_2 and Y_2 are the propagation constant and the characteristic admittance of the hole array and are presented by (4) and (5), respectively. h_2 is the physical height of the array. Y_{s1} and Y_{s3} are the surface admittances at the interfaces between the array and the first and the third regions, respectively, given by (14).

$$\rho_0 = -\frac{1 - \frac{k_z}{\omega\varepsilon_1}\left[\frac{1}{\text{sinc}^2\left(k_x\frac{a}{2\pi}\right)}\frac{\pi^2 d^2}{8a^2}\frac{\beta_2}{\omega\mu_2} + \sum_{m\neq0}\frac{\omega\varepsilon_1}{k_{z,m}}\frac{1}{\text{sinc}^2\left(k_x\frac{a}{2\pi}\right)}\text{sinc}^2\left(k_x\frac{a}{2\pi} + m\frac{a}{d}\right)\right]}{1 + \frac{k_z}{\omega\varepsilon_1}\left[\frac{1}{\text{sinc}^2\left(k_x\frac{a}{2\pi}\right)}\frac{\pi^2 d^2}{8a^2}\frac{\beta_2}{\omega\mu_2} + \sum_{m\neq0}\frac{\omega\varepsilon_1}{k_{z,m}}\frac{1}{\text{sinc}^2\left(k_x\frac{a}{2\pi}\right)}\text{sinc}^2\left(k_x\frac{a}{2\pi} + m\frac{a}{d}\right)\right]} \tag{11}$$

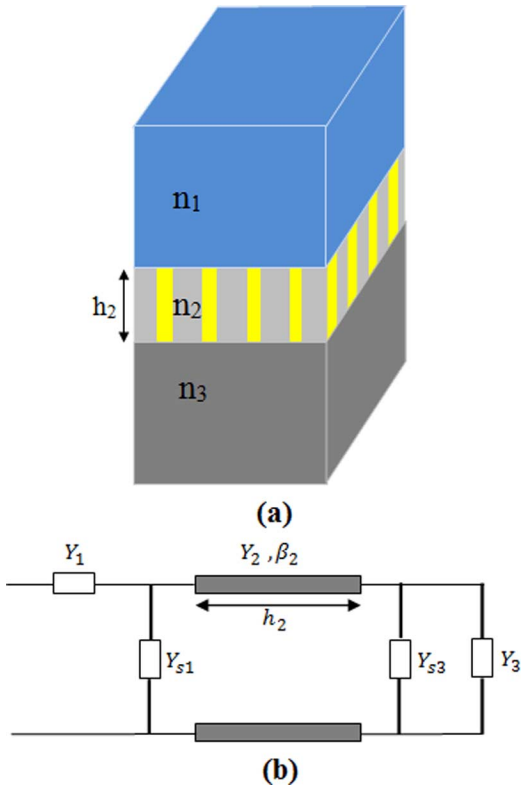

Fig. 3. (a) Periodic metallic hole array filled with silica, located on a silicon substrate and covered by air, and (b) its equivalent circuit model.

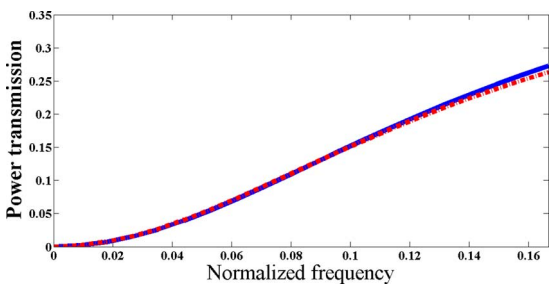

Fig. 4. Power transmission from the structure shown in Fig. 3(a), calculated by CST (solid curve) and the proposed circuit model (dash–dotted curve).

The power transmission of the structure of Fig. 3(a) when illuminated by a normal plane wave is plotted in Fig. 4 versus normalized frequency ($\omega_n = d/\lambda_0$). The results are obtained by using the proposed circuit model (dash–dotted curve) and CST (solid curve). As the figure indicates, the proposed circuit model virtually coincides with the rigorous model.

The required run times of the proposed model and CST on a PC (Intel Core2 i5-2410M CPU @ 2.30 GHz and a 4 GB RAM) are 0.1 s and 40 min, respectively which demonstrates the great advantage of the presented model.

III. Limitations of the Model

It is obvious that the accuracy of the proposed circuit model is limited to the frequency ranges where there is only one propagating mode inside the holes, and only the zeroth diffracted order is propagating outside the hole array.

The condition of having only one propagating mode inside the square holes requires

$$\lambda_0 > \sqrt{2} n_2 (d - W). \tag{15}$$

The condition of having only one propagating diffracted order outside the hole array requires

$$\lambda_0 > d (n_{\max} + n_1 \sin(\theta)) \tag{16}$$

where $n_{\max} = \max\{n_1, n_3\}$.

IV. Transparent Electrode Design

As observed in the previous section, the simpler the simulation method we use, the more efficiently we can design our structures. Thereupon, employing the proposed circuit model, we can design structures with specific features that enable us to use the 2-D arrays of metallic square holes to obtain transparent electrode. As a consequence, we represent two approaches to attain this kind of electrodes. It should be also noted that the metallic structure is thick so the sheet resistance is sufficiently low and will not affected by the optical design.

A. Transparent Electrode Using Binomial Transformer

One of the most indispensable factors that should be taken into account when contriving transparent electrodes is high electromagnetic transmission through the structure. Accordingly, we have employed the structure shown in Fig. 3(a) with $d = 110\ \mu$m to be under normal incidence. In order to efficiently design the structure parameters, we take advantage of the standard binomial transformer[22]. In other words, for the sake of minimizing the reflection from the structure at a specific frequency, we must set the height of the hole array as one fourth of the guided wavelength ($\lambda_g = 2\pi/\beta_2$), and the array's impedance is found to be the geometrical mean of the first and the third regions' impedances at the desired frequency. By obtaining the admittances of the first and third regions from (4), and employing (10) to achieve the admittance of the second region that must be the geometrical mean of the two former admittances, we obtain $W = 10\ \mu$m.

It should be noticed that the normalized frequency range is chosen such that only one diffracted order propagates outside the grating, and the holes support only the dominant eigenmode. In order to achieve maximum sweep within this frequency range, we choose the peak on the power transmission to happen at the middle point of the range which is corresponding to the normalized frequency of $\omega_n = 0.72$. In order to have a maximum power transmission at this normalized frequency, h_2 is obtained to be 21 μm. However, it is noticeable that, due to the surface impedances at the interfaces between the hole array and the upper and lower media, the peak on the power transmission is slightly red-shifted to $\omega_n = 0.6925$.

Fig. 5 shows the power transmission of the discussed structure versus normalized frequency. The solid curve shows CST simulation results when considering the square holes to be perforated in Ag slabs, and the simulation results of the proposed

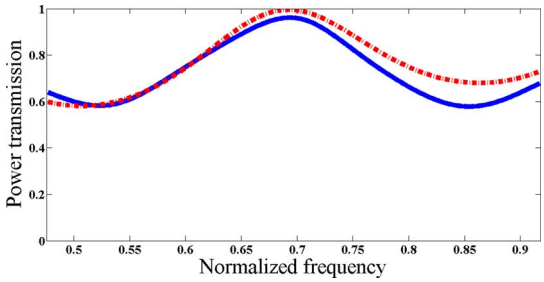

Fig. 5. Power transmission at normal incidence from the structure shown in Fig. 3(a) whose parameters are: $n_1 = 1$, $n_2 = 1.9621$, $n_3 = 3.4205$, $d = 110\,\mu$m, $W = 10\,\mu$m, and $h_2 = 21\,\mu$m. The hole array height is chosen so as to minimize the power reflection from the structure by taking advantage of the standard binomial transformer. CST simulation results are shown by the solid curve, and the results of the analytical model are represented by the dash–dotted curve.

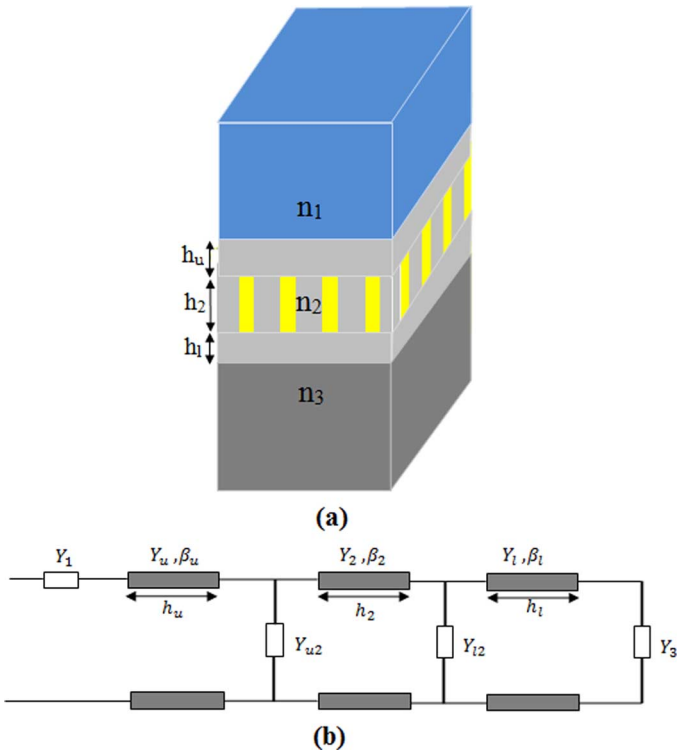

Fig. 6. (a) Structure containing a 2-D array of metallic square holes filled with silica and two silica layers at the top and bottom of the metallic hole array, located on a semi-infinite silicon substrate. (b) Proposed circuit model for the structure of (a).

circuit model by assuming the hole arrays as PEC are depicted by dash–dotted curve.

B. Tri-Layer Transparent Electrode

The other architecture that is designed to realize a transparent electrode with a high transmission is presented in Fig. 6(a). This scheme contains an array of metallic square holes filled with silica with $d = 110\,\mu$m, and two silica layers are inserted at the top and bottom of the hole array. Then, the whole structure is located on a semi-infinite silicon substrate. Fig. 6(b) depicts the proposed circuit model for this architecture in which Y_1, Y_3, Y_u, and Y_l are the admittances of the cover, the substrate, the upper and the lower silica spacer layers, respectively. β_u and β_l

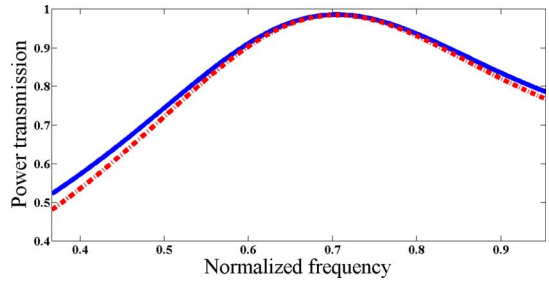

Fig. 7. Power transmission through the structure designed in Fig. 6(a) versus normalized frequency calculated by CST (solid curve) and the proposed circuit model (dash–dotted curve).

represent the propagation constants corresponding to the upper and lower spacer layers and are equal to $k_0 n_2$. Y_{u2} and Y_{l2} are the surface admittances at the interfaces between the array and the upper and lower spacer layers, respectively.

We have four design parameters in this structure: the metal line width (W), the heights of the hole arrays (h_2) and the upper (h_u) and lower (h_l) silica layers. In order to efficiently minimize the power reflection (P_R) over a broad frequency range, at which there is only one propagating diffracted order outside the grating and only the dominant eigenmode is supported by the holes, we minimize the following cost function within the frequency range shown in Fig. 7:

$$CF = \begin{cases} e^{10P_R}, & P_R > 0.15 \\ P_R, & P_R < 0.15 \end{cases} \tag{17}$$

where P_R is the power reflection.

We use the "fminsearch" function of MATLAB for minimizing the cost function. "fminsearch" uses the Nelder–Mead simplex algorithm as described in [23].

The optimization process quickly performed thanks to the availability of analytical expressions for the transmission spectrum of the proposed circuit model.

We numerically find $W = 10\,\mu$m, $h_2 = 10\,\mu$m, $h_u = 6.9\,\mu$m, and $h_l = 10.3\,\mu$m as the optimized structure dimensions. The power transmission through the optimized structure versus the normalized frequency is plotted in Fig. 7. The figure shows the simulation results of CST (solid curve) by using Ag hole arrays, and the proposed circuit model (dash–dotted curve) by assuming PEC square holes.

As illustrated in this figure, the structure has an almost complete power transmission at the normalized frequency of 0.7049. The results also provide evidence to support the claim that the presented structure shows a high level of power transmission (more than 85%) within the normalized frequencies of 0.544 and 0.886 (48% of the central frequency). When compared with the structure proposed in [17] which shows a power transmission of more than 85% within almost 7.5% of the central frequency, the presented optimized structure shows a distinct advantage.

In order to quantify the conductivity of the structure, the concept of sheet resistance is called upon. It is a known fact that the electrical resistance of the block of length L, width W, and thickness t is as follows:

$$R = \frac{\rho}{t}\frac{L}{W} \tag{18}$$

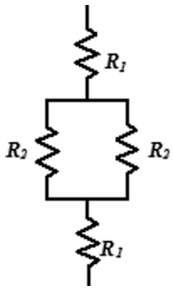

Fig. 8. Simple resistive network that models the electrical resistance of each unit cell of the designed transparent electrode.

where ρ denotes the homogeneous resistivity of the material.

The sheet resistance of the same structure is defined as [24]

$$R_s = R\frac{W}{L}. \tag{19}$$

Finding the sheet resistance of the unit cell of our designed transparent electrode is not that much straightforward. First, it should be noted that the overall electrical resistance of the unit cell when the current flows within the plane of periodicity of the unit cell is to be found via the simple resistive model shown in Fig. 8, where R_1 and R_2 are as follows:

$$R_1 = \frac{\rho}{h_2}\frac{W}{d} \tag{20}$$

$$R_2 = \frac{\rho}{h_2}\frac{d-2W}{W} \tag{21}$$

where d, w, and h_2 are shown in Figs. 1(b) and 3(a).

The overall electrical resistance of the unit cell can then be written as

$$R_{\mathrm{UC}} = \frac{\rho}{h_2}\left(\frac{2W}{d} + \frac{d-2W}{2W}\right). \tag{22}$$

Since the electrical resistance of a block whose width and length are equal to each other is no different from its sheet resistance, and since the width and length of our unit cell are equal to each other, the sheet resistance of the unit cell is no different from R_{UC} in (22). Thanks to the rather large thickness of our proposed transparent electrode ($h_2 = 10\ \mu$m), its sheet resistance is as small as 0.007444 $\Omega/\square$. In contrast, the sheet resistance of the structure presented in [17] is 0.762 $\Omega/\square$. Fortunately, achieving a smaller sheet resistance via our proposed method is not bought at the expense of losing transparency.

V. Conclusion

We proposed an analytical circuit model for 2-D arrays of metallic square holes in order to employ these metamaterials to attain transparent electrodes in terahertz regime. In this circuit model, the bulk of the hole array is replaced by a simple admittance, and the interfaces between the hole array and the homogeneous medium are modeled by a surface admittances which are obtained by employing a mode-matching technique and then comparing the reflection from the structure to the reflection coefficient from the assumed circuit model. The simulation results of the introduced circuit model are in almost complete agreement with the full-wave simulations performed by CST. Accordingly, not only can we simulate the existing architectures containing this kind of metamaterials in a very shorter time compared with the prevalent techniques, but also we can take advantage of this analytical model to design efficient configurations that can be used as transparent electrodes or other required contraptions.

Under these circumstances, we have designed a structure containing 2-D metallic hole arrays to be used as transparent electrode by taking advantage of standard binomial transformer design. Moreover, a tri-layer structure has been designed by using numerical optimization algorithm that shows a power transmission of more than 85% within a wide range of frequencies (48% of the central frequency) which is sufficiently wideband for applications such as solar cells and LEDs. It is noteworthy that we can further increase the desired bandwidth by inserting additional layers.

Appendix

As stated in Section II, the mode-matching technique is used to apply the continuity of the tangential electric and magnetic fields at the discontinuity plane at $\mathrm{z} = 0$. Here, we present the detailed derivation of (11).

Accordingly, continuity of the tangential electric field over the entire unit cell at $\mathrm{z} = 0$ requires that

$$\begin{aligned}&\int_0^d\int_0^d H_1\frac{k_z}{\omega\varepsilon_1}e^{-jk_x x}e^{jk_{x,p}x}dxdy\\ &\quad-\int_0^d\int_0^d\sum_{m=0,\pm1,\pm2,\ldots}\rho_m H_1\frac{k_{z,m}}{\omega\varepsilon_1}e^{-jk_{x,m}x}e^{jk_{x,p}x}dxdy\\ &\quad=\int_0^a\int_0^a E_2\sin\left(\frac{\pi y}{a}\right)e^{jk_{x,p}x}dxdy.\end{aligned} \tag{A1}$$

It should be noted that electric field are multiplied by $e^{jk_{x,p}x}$ and then the integral is taken over the entire unit cell. If $p = 0$:

$$1-\rho_0 = \frac{E_2}{H_1}\frac{2a^2}{\pi d^2}\frac{\omega\varepsilon_1}{k_z}\frac{\sin\left(k_x\frac{a}{2}\right)}{k_x\frac{a}{2}}. \tag{A2}$$

Otherwise, $p \neq 0$ yields to

$$\rho_p = -\frac{E_2}{H_1}\frac{2a^2}{\pi d^2}\frac{\omega\varepsilon_1}{k_{z,p}}\frac{\sin\left(k_{x,p}\frac{a}{2}\right)}{k_{x,p}\frac{a}{2}}. \tag{A3}$$

Along the same line, continuity of the tangential magnetic field over the hole's location and at $\mathrm{z} = 0$ requires that

$$\begin{aligned}&\int_0^a\int_0^a H_1 e^{-jk_x x}\sin\left(\frac{\pi y}{a}\right)dxdy\\ &\quad+\int_0^a\int_0^a\sum_{m=0,\pm1,\pm2,\ldots}\rho_m H_1 e^{-jk_{x,m}x}\sin\left(\frac{\pi y}{a}\right)dxdy\\ &\quad=\int_0^a\int_0^a E_2\frac{\beta_2}{\omega\mu_2}\sin^2\left(\frac{\pi y}{a}\right)dxdy.\end{aligned} \tag{A4}$$

$$\rho_0 = -\frac{1-\frac{k_z}{\omega\varepsilon_1}\frac{1}{\operatorname{sinc}^2\left(k_x\frac{a}{2\pi}\right)}\left[\frac{\pi^2d^2}{8a^2}\frac{\beta_2}{\omega\mu_2}+\sum_{m\neq0}\frac{\omega\varepsilon_1}{k_{z,m}}\operatorname{sinc}^2\left(k_x\frac{a}{2\pi}+m\frac{a}{d}\right)\right]}{1+\frac{k_z}{\omega\varepsilon_1}\frac{1}{\operatorname{sinc}^2\left(k_x\frac{a}{2\pi}\right)}\left[\frac{\pi^2d^2}{8a^2}\frac{\beta_2}{\omega\mu_2}+\sum_{m\neq0}\frac{\omega\varepsilon_1}{k_{z,m}}\operatorname{sinc}^2\left(k_x\frac{a}{2\pi}+m\frac{a}{d}\right)\right]} \tag{A8}$$

Hence

$$H_1\frac{2a^2}{\pi}\left[\frac{\sin\left(k_x\frac{a}{2}\right)}{k_x\frac{a}{2}}(1+\rho_0)+\sum_{m\neq0}\rho_m\frac{\sin\left(k_{x,m}\frac{a}{2}\right)}{k_{x,m}\frac{a}{2}}\right] = E_2\frac{\beta_2}{\omega\mu_2}\frac{a^2}{2}. \tag{A5}$$

Substituting (A3) into (A5), we have

$$(1+\rho_0) = \frac{E_2}{H_1}\frac{k_x\frac{a}{2}}{\sin\left(k_x\frac{a}{2}\right)} \cdot\left[\frac{\pi}{4}\frac{\beta_2}{\omega\mu_2}+\sum_{m\neq0}\frac{2a^2}{\pi d^2}\frac{\omega\varepsilon_1}{k_{z,m}}\left(\frac{\sin\left(k_{x,m}\frac{a}{2}\right)}{k_{x,m}\frac{a}{2}}\right)^2\right]. \tag{A6}$$

Dividing (A6) by (A2) gives

$$\frac{1+\rho_0}{1-\rho_0} = \frac{\frac{k_z}{\omega\varepsilon_1}\left[\frac{\pi^2d^2}{8a^2}\frac{\beta_2}{\omega\mu_2}+\sum_{m\neq0}\frac{\omega\varepsilon_1}{k_{z,m}}\left(\frac{\sin\left(k_{x,m}\frac{a}{2}\right)}{k_{x,m}\frac{a}{2}}\right)^2\right]}{\left(\frac{\sin\left(k_x\frac{a}{2}\right)}{k_x\frac{a}{2}}\right)^2}. \tag{A7}$$

Consequently, the reflection coefficient of the zeroth diffraction order ρ_0 is obtained as (A8), shown at the top of the page.

REFERENCES

[1] D. S. Hecht, L. Hu, and G. Irvin, "Emerging transparent electrodes based on thin films of carbon nanotubes, graphene, and metallic nanostructures," *Adv. Mater.*, vol. 23, no. 13, pp. 1482–1513, 2011.

[2] R. B. H. Tahar, T. Ban, Y. Ohya, and Y. Takahashi, "Tin doped indium oxide thin films: Electrical properties," *Appl. Phys*, vol. 83, no. 5, pp. 2631–2645, 1998.

[3] D. R. Cairns, R. P. Witte, D. K. Sparacin, S. M. Sachsman, D. C. Paine, G. P. Crawford, and R. R. Newton, "Strain-dependent electrical resistance of tin-doped indium oxide on polymer substrates," *Appl. Phys. Lett.*, vol. 76, no. 11, pp. 1425–1427, 2000.

[4] S. Kim, H. K. Yu, K. Hong, K. Kim, J. H. Son, I. Lee, K. B. Kim, T. Y. Kim, and J. L. Lee, "MgO nano-facet embedded silver-based dielectric/metal/dielectric transparent electrode," *Opt. Exp.*, vol. 20, no. 2, pp. 845–853, 2012.

[5] Z. Liu, J. H. Oh, M. E. Roberts, P. Wei, B. C. Paul, M. Okajima, Y. Nishi, and Z. Bao, "Solution-processed flexible organic transistors showing very-low subthreshold slope with a bilayer polymeric dielectric on plastic," *Appl. Phys. Lett.*, vol. 94, no. 20, 2009, Art. ID 203301.

[6] A. T. Mallajosyula, N. Srivastava, S. S. K. Lyer, and B. Mazhari, "Characterization of matrix and isolated organic solar cells," *Sol. Energy Mater. Sol. Cells*, vol. 94, no. 8, pp. 1319–1323, 2010.

[7] P. Kuang, J. M. Park, G. Liu, Z. Ye, W. Leung, S. Chaudhary, D. Lynch, K. M. Ho, and K. Constant, "Metal-nanowall grating transparent electrodes: Achieving high optical transmittance at high incident angles with minimal diffraction," *Opt. Exp.*, vol. 21, no. 2, pp. 2393–2401, 2013.

[8] C. Guillen and J. Herrero, "Influence of the film thickness on the structure,optical and electrical properties of ITO coatings deposited by sputtering at room temperature on glass and plastic substrates," *Semicond Sci. Ech* ., vol. 23, no. 7, 2008, Art. ID 075002.

[9] H. Kim, J. S. Horwitz, G. Kushto, A. Pique, Z. H. Kafafi, C. M. Gilmore, and D. B. Chrisey, "Effect of film thickness on the properties of indium tin oxide thin films," *J. Appl. Phys.*, vol. 88, no. 10, pp. 6021–6025, 2000.

[10] N. F. Anglada, J. P. Puigdemont, J. Figueras, M. Z. Iqbal, and S. Roth, "Flexible, transparent electrodes using carbon nanotubes," *Nanoscale Res. Lett*, vol. 7, no. 1, p. 571, 2012.

[11] B. O'Connor, C. Haughn, K.-H. An, K. P. Pipe, and M. Shtein, "Transparent and conductive electrodes based on unpatterned, thin metal films," *Appl. Phys. Lett.*, vol. 93, no. 22, 2008, Art. ID 223304.

[12] P. Kuang, J. M. Park, W. Leung, R. C. Mahadevapuram, K. S. Nalwa, T. G. Kim, S. Chaudhary, K. M. Ho, and K. Constant, "A new architecture for transparent electrodes: Relieving the trade-off between electrical conductivity and optical transmittance," *Adv. Mater.*, vol. 23, no. 21, pp. 2469–2473, 2011.

[13] A. K. Geim and K. S. Novoselov, "The rise of graphene," *Nature Mater.*, vol. 6, pp. 183–191, 2007.

[14] X. Wang, L. Zhi, and K. Mullen, "Transparent, conductive graphene electrodes for dye-sensitized solar cells," *Nano Lett.*, vol. 8, no. 1, pp. 323–327, 2007.

[15] S. De and J. N. Coleman, "Are there fundamental limitations on the sheet resistance and transmittance of thin graphene films?," *ACS Nano*, vol. 4, no. 5, pp. 2713–2720, 2010.

[16] Y. Wu, X. Ruan, C. H. Chen, Y. J. Shin, Y. Lee, J. Niu, J. Liu, Y. Chen, K. L. Yang, X. Zhang, J. H. Ahn, and H. Yang, "Graphene/liquid crystal based terahertz phase shifters," *Opt. Exp.*, vol. 21, no. 18, pp. 21395–21402, 2013.

[17] R. Malureanu, M. Zalkovskij, Z. Song, C. Gritti, A. Andryieuski, Q. He, L. Zhou, P. U. Jepsen, and A. V. Lavrinenko, "A new method for obtaining transparent electrodes," *Opt. Exp.*, vol. 20, no. 20, pp. 22770–22782, 2013.

[18] O. Luukkonen, C. Simovski, G. Granet, G. Goussetis, D. Lioubtchenko, A. V. Raisanen, and S. A. Tretyakov, "Simple and accurate analytical model of planar grids and high-impedance surfaces comprising metal strips or patches," *IEEE Trans. Antennas & Propag.*, vol. 56, no. 6, pp. 1624–1632, 2008.

[19] A. Khavasi and K. Mehrany, "Circuit model for lamellar metallic gratings in the sub-wavelength regime," *IEEE J. Quantum Electron.*, vol. 47, no. 10, pp. 1330–1335, Oct. 2011.

[20] F. J. Garcia-Vidal, L. Martin-Moreno, and J. B. Pendry, "Surfaces with holes in them: New plasmonic metamaterials," *J. Opt. A, Pure Appl. Opt.*, vol. 7, no. 2, pp. S97–S101, 2005.

[21] M. Naftaly and R. E. Miles, "Terahertz time-domain spectroscopy of silicate glasses and the relationship to material properties," *J. Appl. Phys.*, vol. 102, no. 4, 2007, Art. ID 043517.

[22] D. M. Pozar, *Microwave Engineering*. New York: Wiley, 2011.

[23] J. C. Lagarias, J. A. Reeds, M. H. Wright, and P. E. Wright, "Convergence properties of the Nelder-Mead simplex method in low dimensions," *SIAM J. Optimization*, vol. 9, no. 1, pp. 112–147, 1998.

[24] M. Razeghi, *Technology of Quantum Devices*. Berlin, Germany: Springer, 2009.

Ghazaleh Kafaie Shirmanesh was born in Tehran, Iran, on March 22, 1990. She received the B.Sc. degree in electrical engineering from the Sharif University of Technology, Tehran, Iran, in 2012, where she is currently working toward the M.Sc. degree.

Her current research interests include photonics, circuit modeling of photonic structures, and plasmonics.

Elahe Yarmoghaddam was born in Tehran, Iran, on July 7, 1990. She received the B.Sc. degree in electrical engineering from the Sharif University of Technology, Tehran, Iran, in 2012, where she is currently working toward the M.Sc. degree.

Her current research interests include photonics, circuit modeling of photonic structures, and plasmonics.

Amin Khavasi was born in Zanjan, Iran, on January 22, 1984. He received the B.Sc., M.Sc., and Ph.D. degrees in electrical engineering from the Sharif University of Technology, Tehran, Iran, in 2006, 2008, and 2012, respectively.

He has been an Assistant Professor with the Department of Electrical Engineering, Sharif University of Technology, Tehran, Iran, since 2013. His current research interests include photonics, circuit modeling of photonic structures, and computational electromagnetics.

Khashayar Mehrany was born in Tehran, Iran, on September 16, 1977. He received the B.Sc., M.Sc., and Ph.D. (*magna cum laude*) degrees in electrical engineering from the Sharif University of Technology, Tehran, in 1999, 2001, and 2005, respectively.

He has been an Associate Professor with the Department of Electrical Engineering, Sharif University of Technology, Tehran, Iran, since 2005. His current research interests include photonics, semiconductor physics, nanoelectronics, and numerical treatment of electromagnetic problems.